AN INVESTIGATION INTO THE THERMODYNAMICS OF OVERLAND TROPICAL CYCLONE INTENSITY CHANGE IN WEAKLY/NON-BAROCLINIC ENVIRONMENTS

by

Michael Vossen

A Thesis Submitted in

Partial Fulfillment of the

Requirements for the Degree of

Master of Science

in Atmospheric Science

at

The University of Wisconsin-Milwaukee

August 2021

ABSTRACT

AN INVESTIGATION INTO THE THERMODYNAMICS OF OVERLAND TROPICAL CYCLONE INTENSITY CHANGE IN WEAKLY/NON-BAROCLINIC ENVIRONMENTS

by

Michael Vossen

The University of Wisconsin-Milwaukee, 2021
Under the Supervision of Professor Clark Evans

There are two leading theories regarding how tropical cyclones can maintain or increase their intensity over land in weakly to non-baroclinic environments. In the first, tropical cyclones are maintained overland by enhanced upward surface enthalpy fluxes facilitated by the tropical cyclone's rains, whereas in the second, tropical cyclones are maintained by enhanced enthalpy fluxes under inflowing trajectories at larger radii from the cyclone's center. These theories have yet to be rigorously tested, however. To rigorously test these hypotheses, this study uses a quasi-idealized version of the Weather Research and Forecasting model lacking parameterized radiation to test the sensitivity of overland tropical cyclone intensity to the underlying land surface's characteristics. In these simulations, the coldest initial land surfaces result in the strongest simulated tropical cyclones after landfall as they are associated with a negative sensible heat flux that creates a nighttime-like near-surface temperature inversion. This nighttime-like inversion suppresses tropical cyclone rainband activity, preventing lower equivalent potential temperature air from the midtroposphere from being mixed into the inflowing near-surface trajectories by convective downdrafts. The results do not fully support either of the two leading hypotheses and further investigations are needed to address shortcomings in the applicability of this study's findings to observed events.

TABLE OF CONTENTS

LIST OF FIGURES

LIST OF TABLES

ACKNOWLEDGEMENTS

First and foremost, I want to thank my advisor Dr. Evans for his help with advising me though this project and giving me the chance to study atmospheric science here at the University of Wisconsin-Milwaukee.

Also, thank you to Dr. Roebber and Dr. Kahl for serving on my thesis committee.

Lastly, thank you to my family, friends, and fellow classmates who have been a tremendous help with their support on this project.

1. Introduction

Tropical cyclones (TCs) typically decay as they hit land, first because of increased surface roughness and subsequently because of the reduced ability to extract enthalpy from the underlying land surface (e.g., Tuleya 1994, Chen and Chavas 2020, Hlywiak and Nolan 2021). However, recent studies suggest that it is possible for tropical cyclones to maintain themselves or even intensify following landfall in non- and weakly baroclinic environments (e.g., Tuleya 1994, Shen et al. 2002, Emanuel et al. 2008, Evans et al. 2011, Anderson and Shepherd 2014, Chen and Chavas 2020, Yoo et al. 2020, Hlywiak and Nolan 2021). Notable cases of tropical cyclones maintaining or intensifying over land include Abigail (2001; Emanuel et al. 2008), Erin (2007; Arndt et al. 2009; Monteverdi and Edwards 2010; Evans et al. 2011; Kellner et al. 2011), and Kelvin (2018; Yoo et al. 2020). The largest number of overland TC maintenance or intensifying events are found over northern Australia (Emanuel et al. 2008, Anderson and Shepherd 2014, Yoo et al. 2020).

Over the ocean, it is well known that tropical cyclones gain energy from surface enthalpy fluxes (Riehl 1950, Kleinschmidt 1951, Emanuel 2018). This combination of surface sensible and latent heat fluxes is then used to warm and moisten the air moving towards the center of the tropical cyclone. Generally speaking, the heating from surface sensible heat fluxes offsets the adiabatically cooling air as air moves from high pressure to low pressure immediately above the surface. At the same time there is also an isothermal expansion of the air as it warms, allowing the tropical cyclone's minimum sea-level pressure to decrease (Riehl 1950). As the minimum sea-level pressure decreases, the air's saturated vapor pressure increases. Alone, this would result in lower relative humidity near the surface; however, a constant high relative humidity is maintained by upward-directed surface latent heat fluxes (Ooyama 1969). Both soil and oceans

can facilitate these enthalpy fluxes, but one difference that soil has from the ocean is that soil generally cannot sustain these surface enthalpy fluxes as long or as strongly as the water in the ocean due to land's relatively low heat capacity and thermal conductivity (Tuleya 1994). This low heat capacity can be overcome by adding water to the land surface, such as that present in shallow water bodies such as wetlands and lakes (Shen et al. 2002). Another difference between the ocean and land is that land has a higher surface roughness. Land surfaces with higher surface roughness result in tropical cyclones decaying faster upon landfall than land surfaces with low surface roughness (Chen and Chavas 2020, Hlywiak and Nolan 2021).

Theories on tropical cyclone maintenance and intensification over land start to diverge when it comes to partially wetted soils with no standing water, however. One theory, first advanced by Emanuel et al. (2008) and later colloquially known as the "brown-ocean effect" (Andersen and Shepherd 2014), emphasizes the role of surface latent heat fluxes directly beneath a tropical cyclone over land. This theory, initially based on idealized-model simulations of tropical cyclones over hot, sandy soils, begins with the underlying soil being wetted by the tropical cyclone's rain. This rainfall causes the upper soil, or substrate, to cool. With the lower substrate being unaffected by the rain and warmer than the now-cooled upper substrate, a positive vertical temperature gradient is created in the soil. Gradually the heat from the lower substrate works its way up to the upper substrate. The re-warming of the upper substrate plus the addition of soil moisture from the initial rains allows for greater upward surface enthalpy fluxes from the upper substrate to the lower atmosphere than before the rain and to maintain the upward surface enthalpy fluxes longer than when the soil is dry. The larger upward surface enthalpy fluxes are sometimes large enough to maintain the tropical cyclone. This process continues as the tropical cyclone moves inland, but the impact it can have diminishes as the tropical cyclone

moves inland and further away from the large-scale moisture supply from the ocean environment, which decreases the tropical cyclone's ability to produce the necessary rainfall (Emanuel et al. 2008, Andersen et al. 2013, Andersen and Shepherd 2014).

A second theory, first advanced by Evans et al. (2011), emphasizes large-scale near-surface moisture transport and surface enthalpy fluxes along inflowing trajectories, rather than directly underneath a tropical cyclone, in facilitating tropical cyclone maintenance and intensification over land. Based on a case study of tropical storm Erin (2007) over the south-central United States, this theory says that maintaining initially high environmental boundary layer moisture over land is important for tropical cyclone maintenance. This boundary layer moisture is maintained by upward surface enthalpy fluxes along inflowing trajectories that pass over a land surface with an abnormally high soil moisture content. The theory proposed by Emanuel et al. (2008) is not completely ruled out in the Evans et al. (2011) theory but is deemed a secondary process rather than a primary process. Another important difference between the two theories is the location of the study: the primarily sandy soils of northern Australia versus the primarily clay-like soils of the south-central United States. These two different soils have different heat capacities and thermal conductivities, each of which have been shown to impact tropical cyclone maintenance and intensification over land (Tuleya 1994).

However, both theories have limitations arising from the methodologies used in developing each of them. The first theory is based on highly idealized model simulations, with simplified and somewhat unrealistic representations of physical processes (e.g., the atmosphere being hydrostatically balanced, soil moisture being only saturated or dry, enthalpy fluxes being dependent on land elevation, vertical wind shear effects being completely omitted, and the tropical cyclone having to be manually moved rather than the steering flow moving the tropical

cyclone). Conversely, the second theory is largely based on a single full-physics real-data numerical-model case study of a single event that occurred outside of the climatologically favored location for non- to weakly baroclinic overland tropical cyclone intensification. While facilitating the development of novel understanding, case studies incorporate substantial atmospheric variability and non-linearity, imperiling the ability to reliably discern physical causalities. Further, given their focus on a limited number of cases with a limited number of simulation configurations, case-study analyses are not always generalizable to a wider range of cases.

Based on the gaps in non- to weakly baroclinic overland tropical cyclone maintenance knowledge discussed, this study aims to test two different hypotheses. The first hypothesis is that hot, wet, sandy soils have the greatest ability (relative to other soil types, such as clay, loam, and rock, as well as soil temperature and moisture content) to have upward-directed surface enthalpy fluxes large enough to maintain or intensify tropical cyclones over land in non- or weakly baroclinic environments. The second hypothesis is that remote surface enthalpy fluxes (rather than those directly under the tropical cyclone) are the primary but not exclusive driver of tropical cyclone maintenance and intensification over land. A series of quasi-idealized numerical simulations is used to rigorously test these hypotheses.

A detailed description of the methods used to build the idealized simulations is presented in section 2, followed by an analysis of the results from these models in section 3. Finally, a summary of the results and conclusions is presented in section 4.

2. Methods

a. Model configuration

A quasi-idealized version of the Advanced Research version of the Weather Research and Forecasting model (WRF-ARW; Skamarock et al. 2019), version 4.1.3, is used to test the two hypotheses underpinning this study. WRF-ARW contains an idealized configuration specifically for tropical cyclones, but this is not used in the simulations presented in this study because it is overly limiting to the user in how it can be configured. For example, the idealized configuration requires that any desired changes to the ocean and land conditions (e.g., temperature, moisture fraction, and soil type) be made through changing the source code, which requires recompiling the model each time it is used. A second issue with the idealized approach is that radiation cannot be included in the simulation. An alternative approach is given by a quasi-idealized model configuration, which permits idealized simulations using the real-data WRF-ARW framework (e.g., Hill and Lackmann 2009). This quasi-idealized configuration provides more flexibility in adding and removing features such as vertical wind shear, parameterized physical processes, and terrain that may impact the tropical cyclone, allowing for the simulations' complexity to gradually build from highly idealized to full physics.

To properly test the proposed hypotheses, the model domain encompasses 1200 x 1100 x 50 grid points, with 3 km lateral grid spacing, 50 vertical levels with eight under the 0.9 hybrid sigma-pressure vertical level (approximately 1 km above ground level), and a model top of 50 hPa. Model parameterizations largely follow those of the Advanced Hurricane WRF (Davis et al. 2008) configuration and include the Yonsei University planetary boundary layer parameterization (Hong et al. 2006), Thompson microphysics parameterization (Thompson et al. 2008), the revised MM5 similarity surface layer parameterization (Jimenez et al. 2012), and

Noah land-surface model (LSM; Chen and Dudhia 2001) with four soil levels centered at 0.05, 0.25, 0.7, and 1.5 m. Radiation is not used in the primary simulations reported on in this study to allow for fewer degrees of freedom in the response to the changing soil conditions. All simulations are initialized with a land surface that is $7/12^{th}$ ocean to the west and $5/12^{th}$ land to the east (Fig. 1). The ocean temperature is set to a constant 300 K for the duration of every simulation. All simulations are conducted on a *f*-plane at 22°S, chosen as it passes through the climatologically favored non- or weakly baroclinic overland tropical cyclone maintenance regions of northern Australia (Andersen and Shepherd 2014). The atmosphere is initialized with the Dunion (2011) moist tropical sounding with vertically uniform 5 m s^{-1} westerly winds, the latter of which ensures that a tropical cyclone initialized over water is directed toward land over time. The combination of horizontally homogeneous initial atmospheric conditions with no vertical wind shear results in a non-baroclinic initial atmospheric state. Lateral boundary conditions are prescribed and are set to the Dunion (2011) moist tropical sounding with vertically uniform 5 m s^{-1} westerly winds throughout the simulation. Finally, a synthetic tropical cyclone is initialized using the WRF-ARW tropical cyclone bogus scheme (Davis and Low-Nam 2001) at the location shown in Fig. 1 with an initial maximum 10-m wind speed of 30 m s^{-1} and a 150-km radius of maximum winds. The model is integrated forward once for 24 h with a default soil condition of 300 K initial soil temperature, 0.4 initial soil moisture fraction, and silty clay loam soil, to allow for realistic hydrometer, wind fields, and temperature fields to form with the synthetic tropical cyclone while it remains over water (Fig. 2).

A total of twenty-seven simulations are conducted, with each varying in their initial soil temperature, soil moisture fraction, and soil type as shown in Table 1. Soil parameter permutations are chosen in a way to test the main soil conditions over which tropical cyclones

have and have not been observed to intensify (Andersen and Shepherd 2014) to find the soil characteristics that are the most favorable for overland weakly or non-baroclinic tropical cyclone maintenance and intensification. Specifically for the soil temperatures, 310 K is chosen to represent a soil temperature representative of northern Australia's summer daytime soil temperatures, 300 K is chosen to represent an equilibrium between the soil temperatures and the surface air temperature of the Dunion (2011) moist tropical sounding, and 295 K is chosen to represent a soil temperature representative of northern Australia's summer nocturnal soil temperatures. Each simulation is initialized at the end of the 24 h synthetic tropical cyclone initialization period with one combination of adjusted soil conditions at all four soil levels and then integrated forward another 72 h.

b. Trajectory Analysis

A trajectory analysis is performed for all twenty-seven soil sensitivity simulations using the Lagrangian Analysis Tool (LAGRANTO; Miltenberger et al. 2013). Backward trajectories are released at the final time (72 h) in each simulation from a 500 x 500 km matrix centered on the tropical cyclone's sea-level pressure minimum with 50 km lateral spacing and an altitude of 100 m above ground level. Trajectory positions are updated every hour, matching the WRF-ARW simulations' output frequency. Backward trajectory positions and attributes are not sensitive to their starting altitudes (within the range 75-125 m) or initialization time (within the range 66-72 h; both not shown). Furthermore, forward trajectories released from the backwards trajectories' ending locations approximately return to the backward trajectories' starting locations, suggesting there is little sensitivity of the trajectories to the highly curved convergent low-level flow (e.g., Dahl et al. 2012) with the simulated tropical cyclones.

Soil Conditions Used

Soil Type	Silty Clay Loam, Sand, Rock
Initial Soil Temperature (K)	310, 300, 295
Initial Soil Moisture Fraction (non-dimensional)	0.4, 0.25, 0.1

Table 1. Soil conditions used in the soil sensitivity simulations.

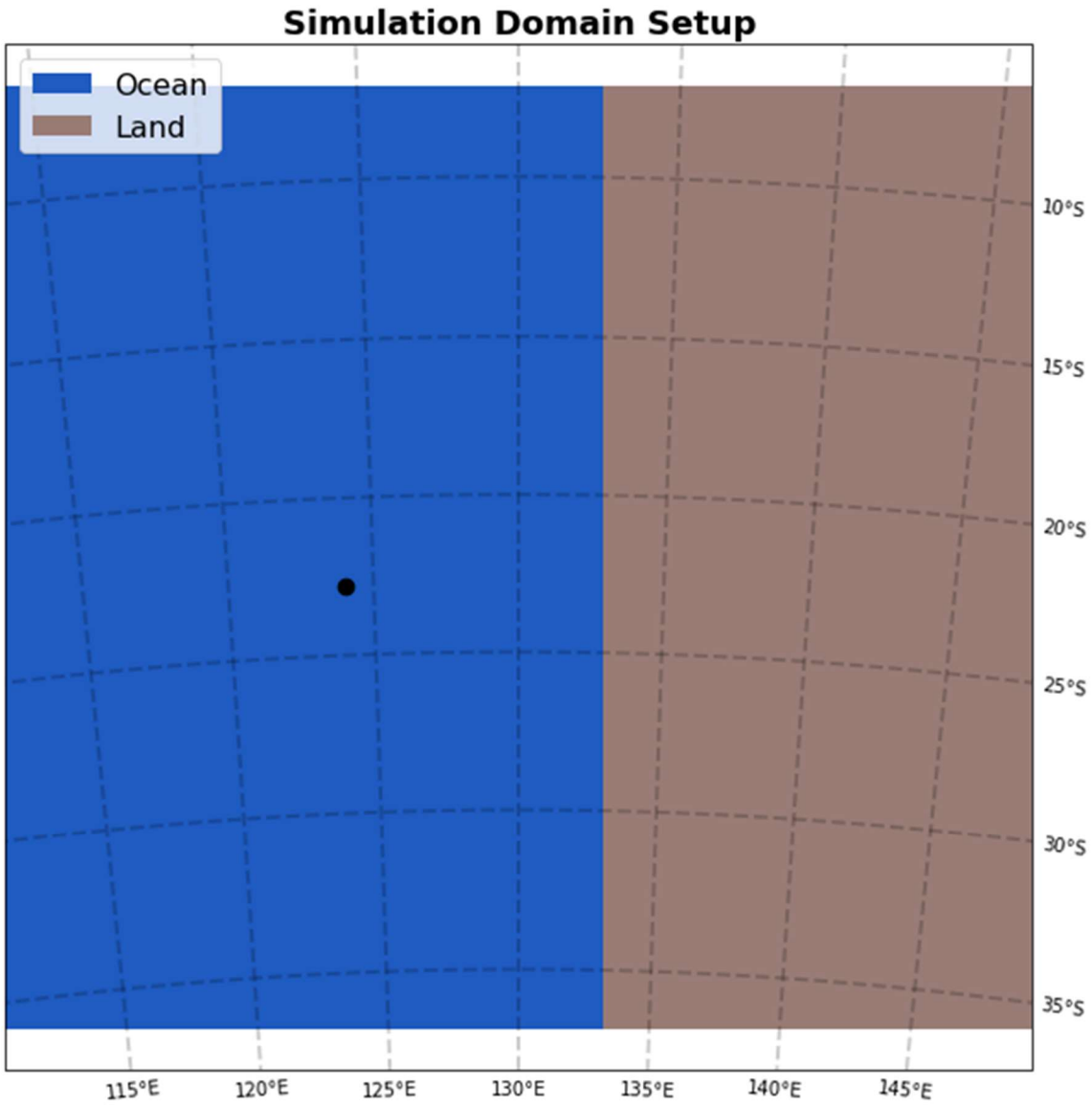

Figure 1. Model land-surface, with brown indicating land and blue indicating ocean. The black dot over the ocean indicates the tropical cyclone's initialization location.

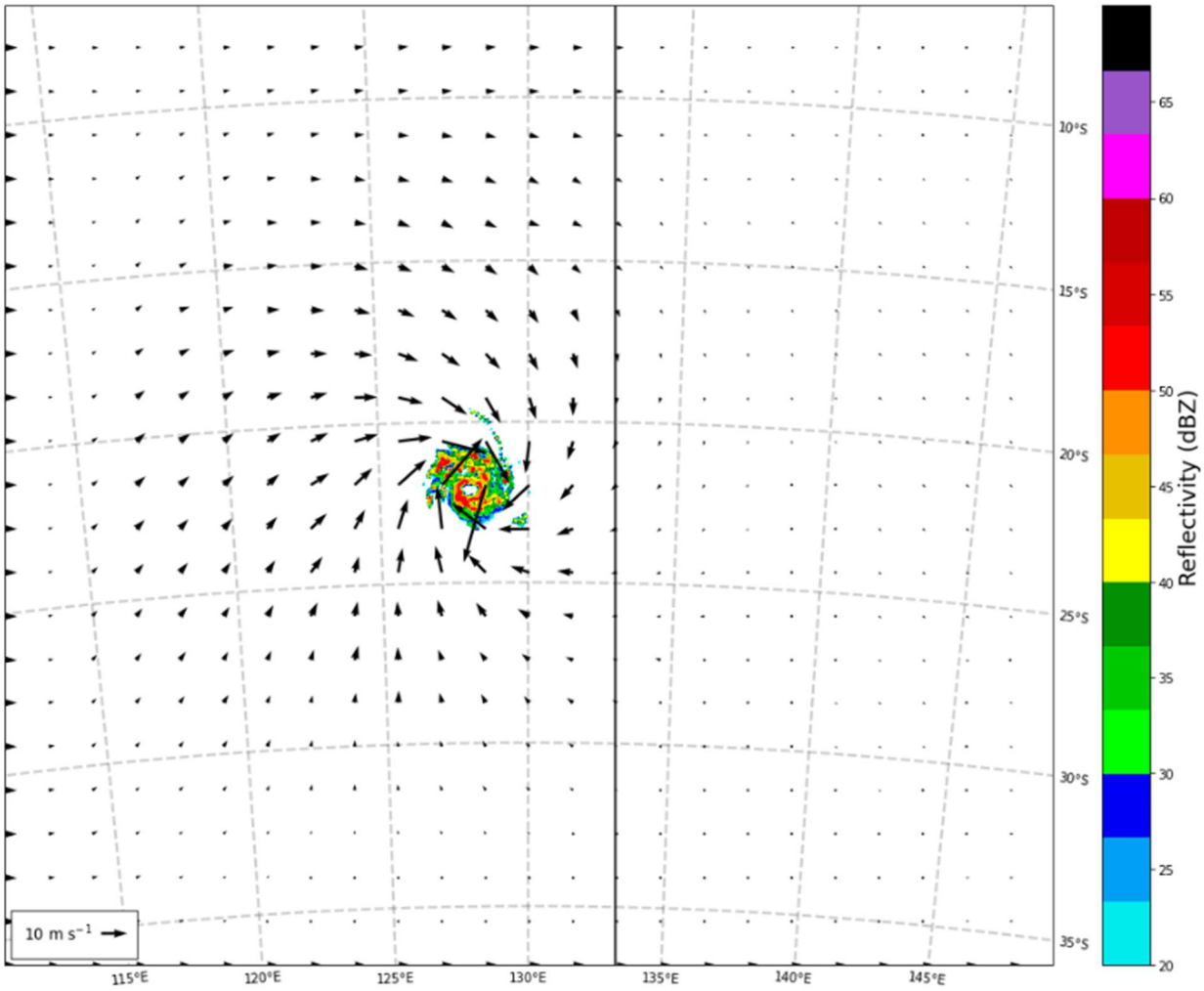

Figure 2. Simulated tropical cyclone 10-m horizontal wind (vectors) and 1-km above ground level 10-cm reflectivity (dBZ; shaded) 24 h after initializing the synthetic tropical cyclone.

3. Results

Each simulation produces a simulated tropical cyclone with a peak intensity (from hourly outputs) equivalent to a high category 2 or a low category 3 on the Saffir-Simpson hurricane wind scale (National Hurricane Center 2021) at about 15 h after restarting the simulation with updated soil parameters (Fig. 3). After this time, all of the simulated tropical cyclones start to rapidly weaken and continue to do so after making landfall at approximately 25 h. Even after landfall, however, the simulated tropical cyclones maintain a warm-core structure, with radial potential temperature anomalies that are largest at mid-levels near their centers (Fig. 4).

Once inland, only tropical cyclones with the silty clay loam land surface exhibit a weak relationship to initial soil moisture fraction variations (Fig. 3). Both the sand and the rock simulations show no response to the changing soil moisture. This is because the rock and sand simulations lose their soil moisture early in the simulations when a high soil moisture fraction is prescribed (Fig. 5) due to their low porosity and field capacity (Table 2). These lower porosities and field capacities cause the soil moisture to drain out quickly to a lower soil moisture fraction that the soil physically can hold. For the rock and sand simulations, the field capacity is less than the initially prescribed 0.4 and 0.25 soil moisture fractions, such that soil moisture rapidly decreases to values closer to their respective field capacities.

In contrast, there are clearer distinctions between the simulations with different initial soil temperatures. Some small intensity differences exist prior to landfall, with the simulated tropical cyclones in the warmest initial soil temperature simulations weakening faster than the coldest initial soil temperatures (Fig. 6). Initially following landfall, however, these simulated tropical cyclones weaken at a slower rate than the cold soil temperatures. Around 42 h, some of the simulated tropical cyclones in the simulations initialized with colder soil temperatures (for all

soil types) begin to maintain or even increase their intensity (Fig. 6). In contrast, the simulated tropical cyclones in most simulations with intermediate initial soil temperatures and all simulations with the warmest initial soil temperatures (for all soil types and initial soil moisture fractions) continue a slow decay after this time. Note that additional simulations with random finite perturbations to the initial atmospheric conditions produce similar results, suggesting that this relationship to the initial soil temperature is at least partially insensitive to the simulations' initial conditions (not shown).

Corresponding to the intensity response to initial soil temperature variations are differences in the simulated tropical cyclones' precipitation fields. Specifically, the simulations with the coldest initial soil temperatures consistently are associated with less outer rainband activity than in all but one intermediate initial soil temperature simulation (not shown) and in all simulations with the warmest initial soil temperatures (Figs. 7-8). Thus, a correspondence exists between outer rainband extent and post-landfall tropical cyclone intensity. In the simulations with extensive outer rainbands, the radially averaged diabatic warming is not concentrated near the simulated tropical cyclone's center (Fig. 9a) and thus can only result in a small sea-level pressure decrease over a broad area. In the simulations where the precipitation is centralized near the simulated tropical cyclones' centers, however, diabatic heating is confined near the center (Fig. 9b) where it can result in a larger sea-level pressure decrease.

One possible explanation for the relationship between outer rainband coverage and initial soil temperature is the environmental atmospheric boundary-layer stability. Simulations with initially warmer soil temperatures are associated with a shallow surface-based mixed layer with minimal surface-based convective inhibition (CIN; Figs. 10a,c,e) whereas simulations with initially colder soil temperatures are associated with a shallow surface-based inversion with

larger surface-based CIN (Figs. 10b,d,f). The origins of these difference stem from the profile used and the prescribed soil temperatures. The Dunion (2011) moist tropical sounding used to initialize the atmosphere has a surface air temperature of 300 K whereas the land in the warmest simulations has an initially prescribed soil temperature of 310 K. In the absence of radiation, these simulations are *generally* associated with a positive (i.e., upward) surface sensible heat flux over land (Figs. 11a,c,e), resulting in dry convection, turbulent vertical mixing, and surface-based mixed layer development (Figs. 10a,c,e). On the other hand, in the coldest simulations the initial soil temperature is prescribed as 295 K, or 5 K colder than the initially prescribed surface air temperature. In the absence of radiation, these simulations are *generally* associated with a negative (i.e., downward) surface sensible heat flux over land (Figs. 11b,d,f), resulting in a shallow near-surface temperature inversion (Figs. 10b,d,f). Thus, the soil's initial surface temperature dictates how much surface-based CIN is present in the environment (in the absence of radiation), which ultimately dictates the extent of the tropical cyclone's outer rainbands. The larger surface-based CIN works against outer rainband formation by inhibiting ascent away from the strongly forced ascent (due to large-scale convergence) near the tropical cyclones' centers.

Along with suppressing outer rainbands, colder initial soil temperatures decrease the near-surface equivalent potential temperature (through negative surface sensible heat fluxes) of inflowing air parcels, providing less energy to fuel the tropical cyclone relative to the initial atmospheric condition. Conversely, warmer initial soil temperatures increase the near-surface equivalent potential temperature of inflowing air (through near-zero to positive surface sensible heat fluxes), increasing the energy available to fuel the tropical cyclone relative to the initial atmospheric condition. However, with more rainbands present in the warmer initial soil temperature simulations, there is more opportunity for lower equivalent potential temperature air

to be flushed by convective downdrafts from the midtroposphere down toward the surface (Powell 1990). In the simulations with the warmest initial soil temperatures, a subset of trajectories that ultimately end up near the simulated tropical cyclone's center at low levels originate in the midtroposphere (Fig. 12). On the way to the simulated tropical cyclone's center, these trajectories are entrained into the outer rainbands (Fig. 13). These trajectories descend through outer rainband downdrafts, bringing low midtropospheric equivalent potential temperature air into the boundary layer (Figs. 13a,c,e). As these trajectories subsequently advect toward the tropical cyclone's center, the low thermal conductivities of the underlying soil (relative to water; Tuleya 1994, Shen et al. 2002) result in the soil being unable to transfer sufficient enthalpy to the inflowing air, resulting in weaker deep moist convection, weaker diabatic heating, and thus a weaker simulated tropical cyclone than in the simulations with colder initial soil temperatures. Conversely, in the simulations with the coldest initial soil temperatures, nearly all trajectories start and remain near the surface as they flow inward toward the simulated tropical cyclone's center (Fig. 14). Although these inflowing trajectories do experience a small reduction in equivalent potential temperature due to a negative surface sensible heat flux, they nevertheless maintain a higher equivalent potential temperature (Fig. 12b,d,f) than do their counterparts in the warmer initial soil temperature simulations. Thus, simulations with initially colder soil temperatures allow air with comparatively high equivalent potential temperature to reach the simulated tropical cyclone's center near the surface, whereupon its enthalpy is released in a centralized zone of diabatic warming in the middle to upper troposphere.

Soil Type	Porosity	Field Capacity	Thermal Conductivity Coefficient
Silty Clay Loam	0.464	0.387	-1.118
Sand	0.339	0.192	-0.472
Rock	0.20	0.17	-1.111

Table 2. Soil characteristics for each soil type prescribed in the simulations conducted. Values for each soil type are the values used by the Noah LSM. Porosity is defined as the amount of water that can be stored in a volume of soil, whereas the field capacity is defined as the amount of water that can be held by a soil after drainage has ceased (Cornell 2010).

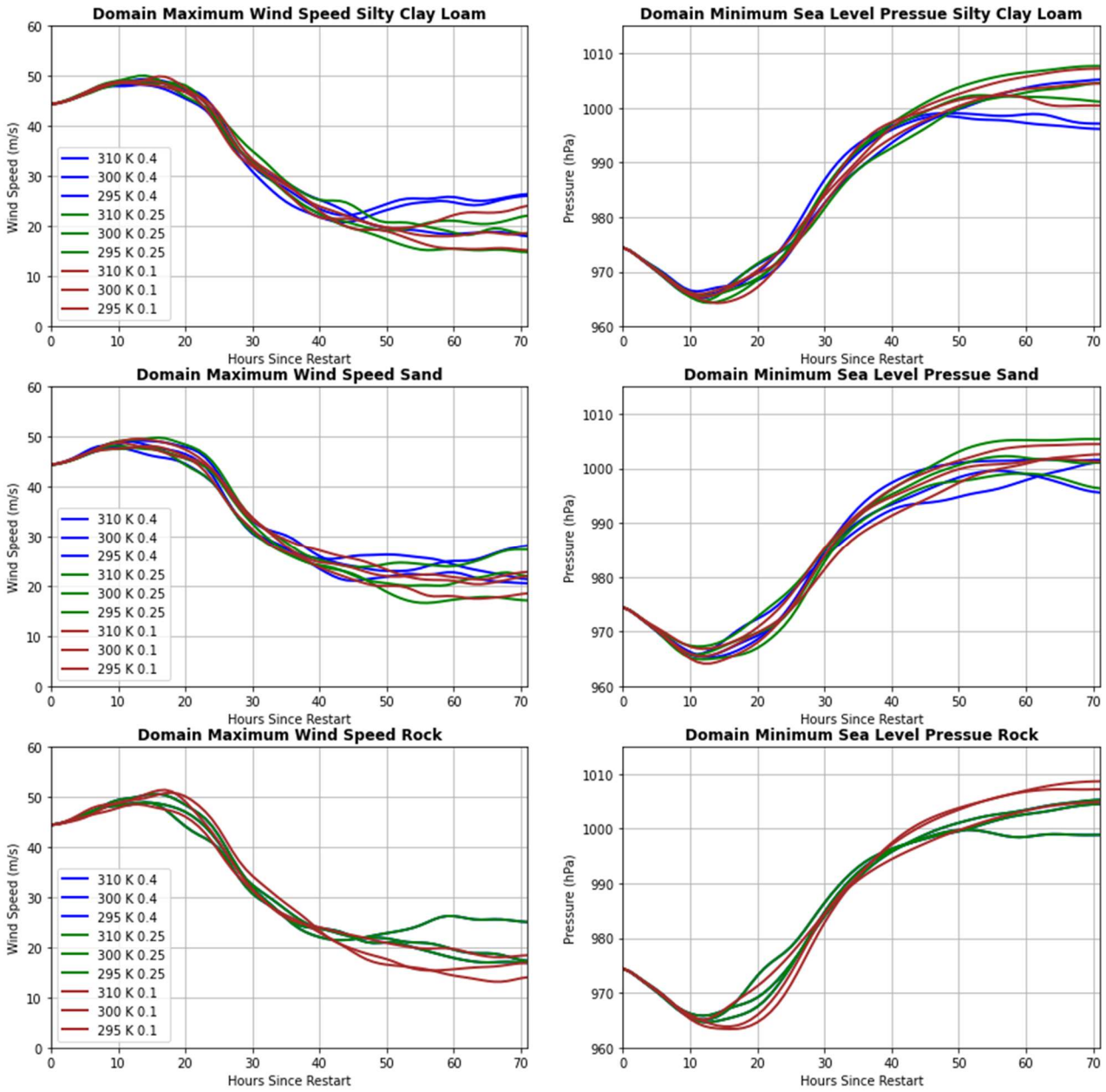

Figure 3. Domain-maximum 10-m wind speed (m s^{-1}; left panels) and domain-minimum sea level pressure (hPa; right panels) for the (top) silty clay loam, (middle) sand, and (bottom) rock simulations. Blue lines indicate the simulations with the highest initial soil moisture fraction (0.4), green lines indicate the simulations with an intermediate initial soil moisture fraction (0.25), and the brown lines indicate the simulations with the driest initial soil moisture fraction (0.1).

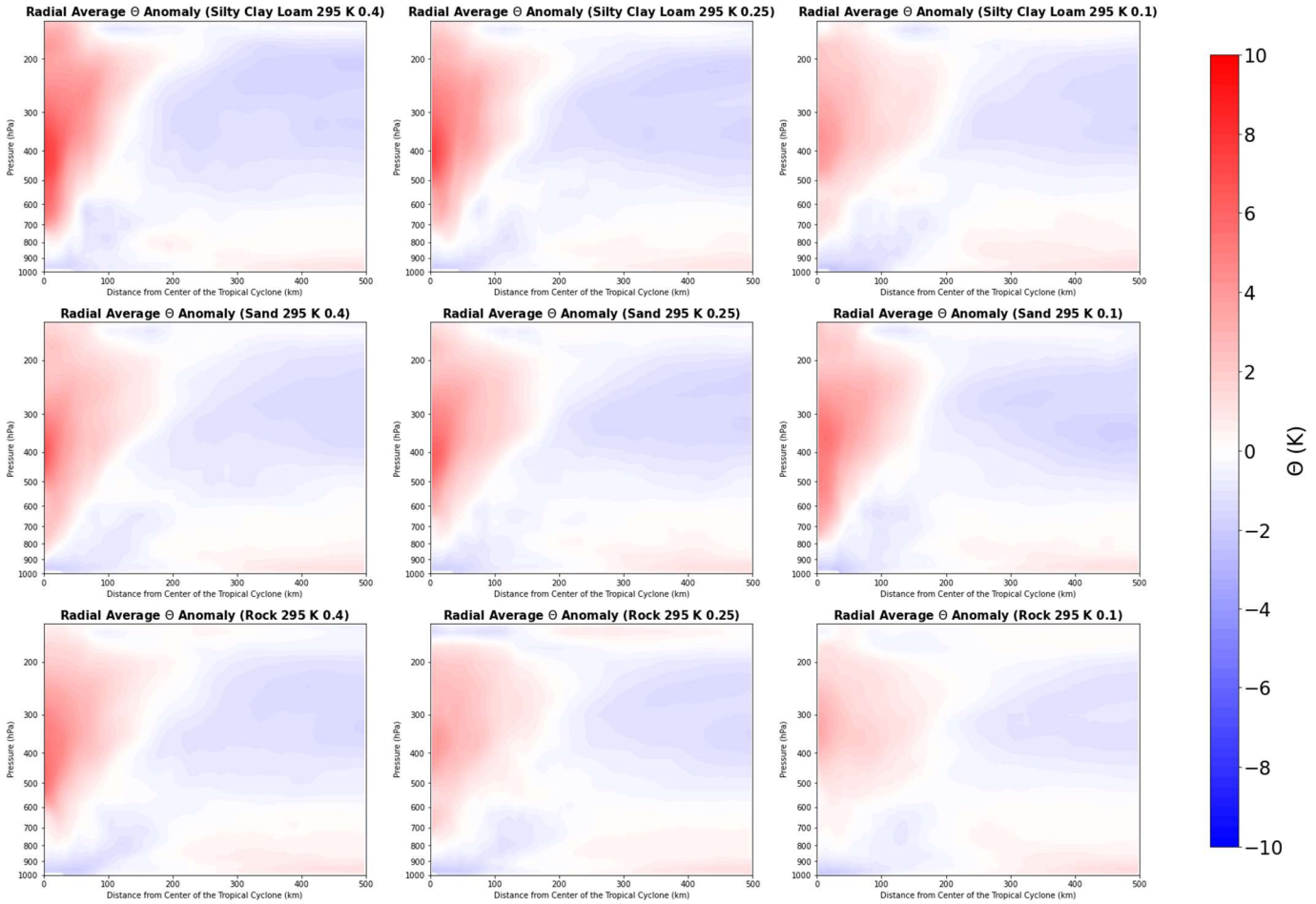

Figure 4. Radially averaged potential temperature anomalies (from the radial mean; shaded, units: K) for the simulations using an initial 295 K soil temperature. The top, middle, and bottom rows depict the silty clay loam, sand, and rock simulations, respectively, while the left, center, and right columns depict the simulations with initial soil moisture fractions of 0.4, 0.25, and 0.1, respectively.

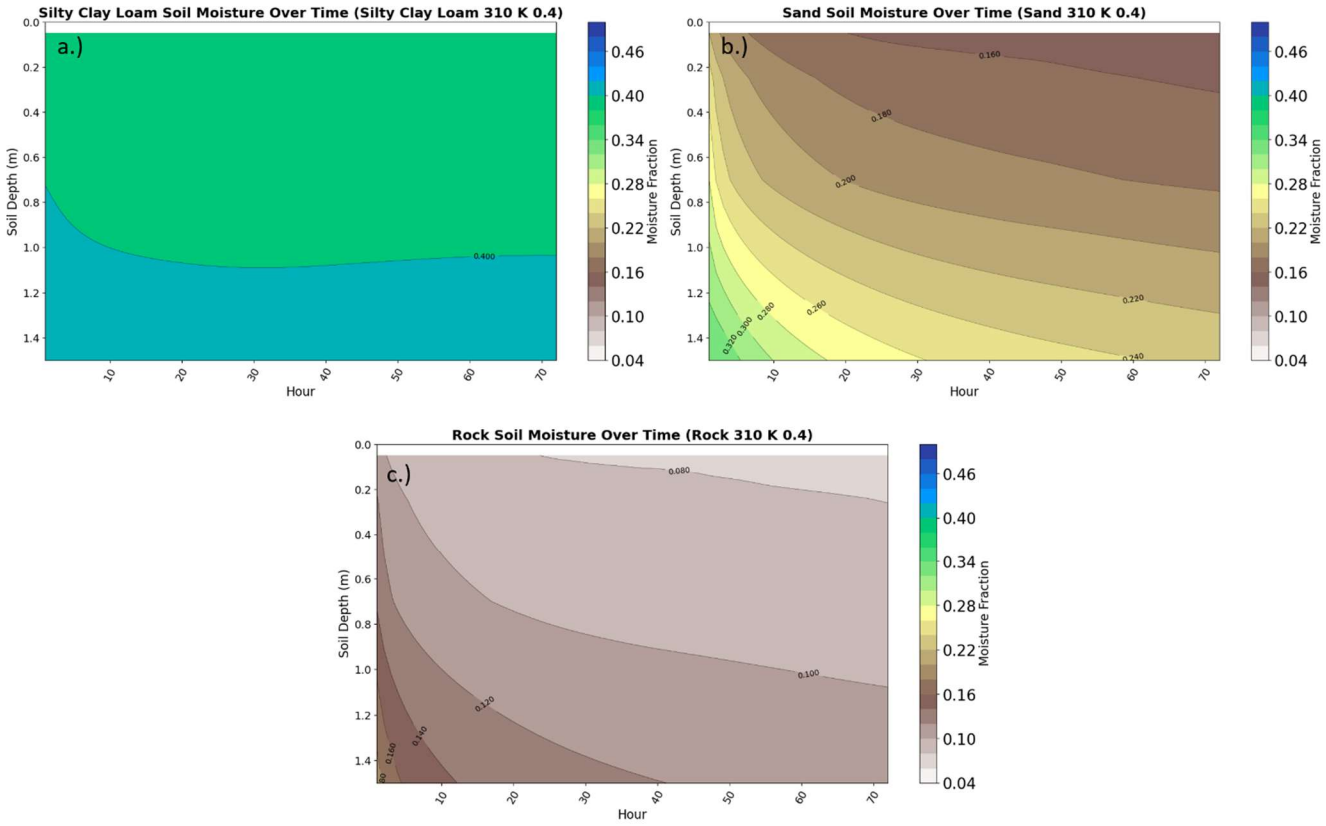

Figure 5. Domain-averaged soil moisture fraction (nondimensional) as a function of soil depth (*y*-axis) and time (*x*-axis) for the simulations with an initial 310 K soil temperature and 0.4 soil moisture fraction. The top panel is the silty clam loam land surface, the center panel is the sand land surface, and the bottom panel is the rock land surface.

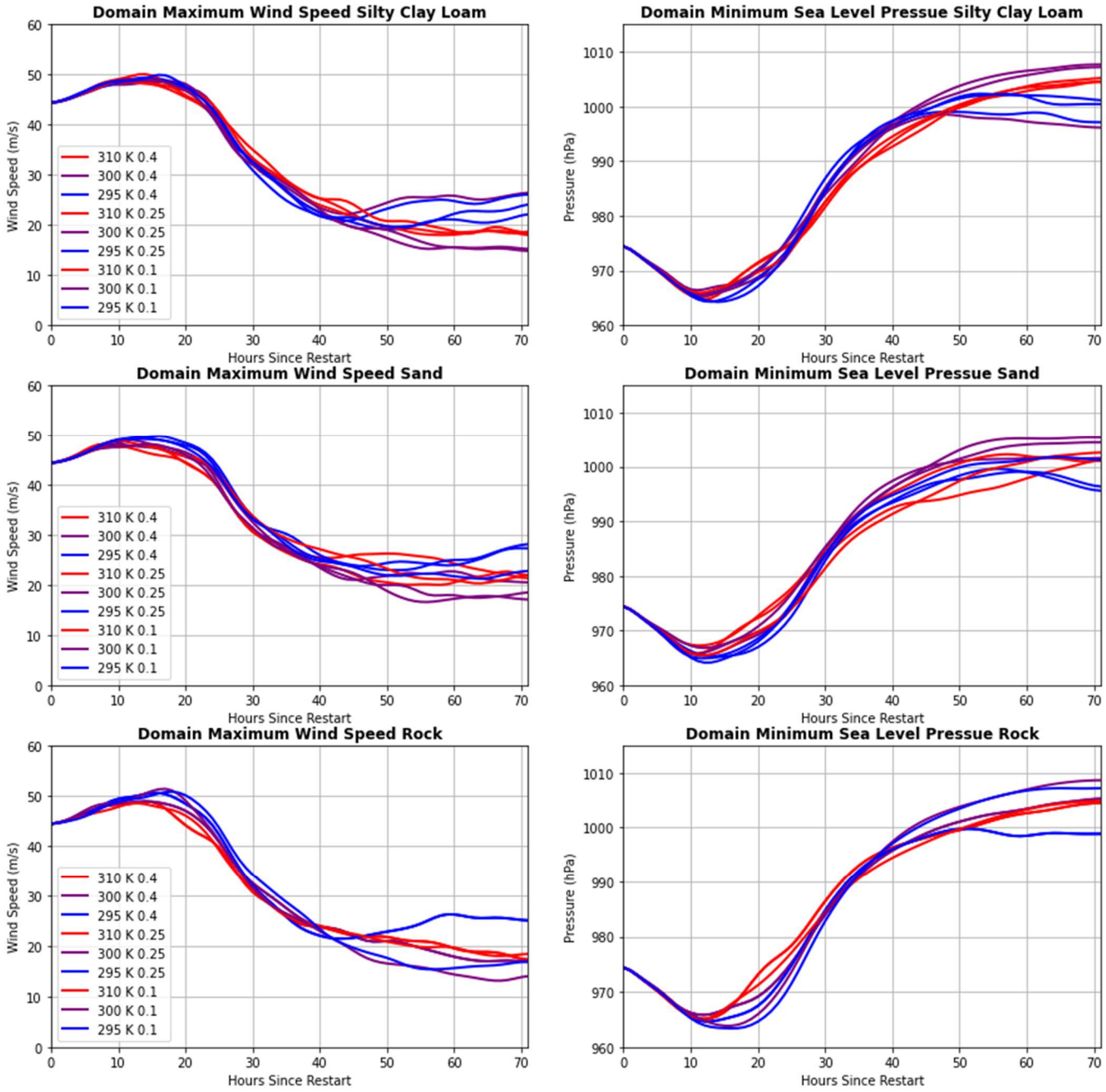

Figure 6. As in Fig. 4, except with lines colored to show the intensity differences between simulations with varying initial soil temperatures. Red lines indicate the simulations with the warmest initial soil temperatures (310 K), purple lines indicate the simulations with an intermediate initial soil temperature (300 K), and blue lines indicate the simulations with the coldest initial soil temperatures (295 K).

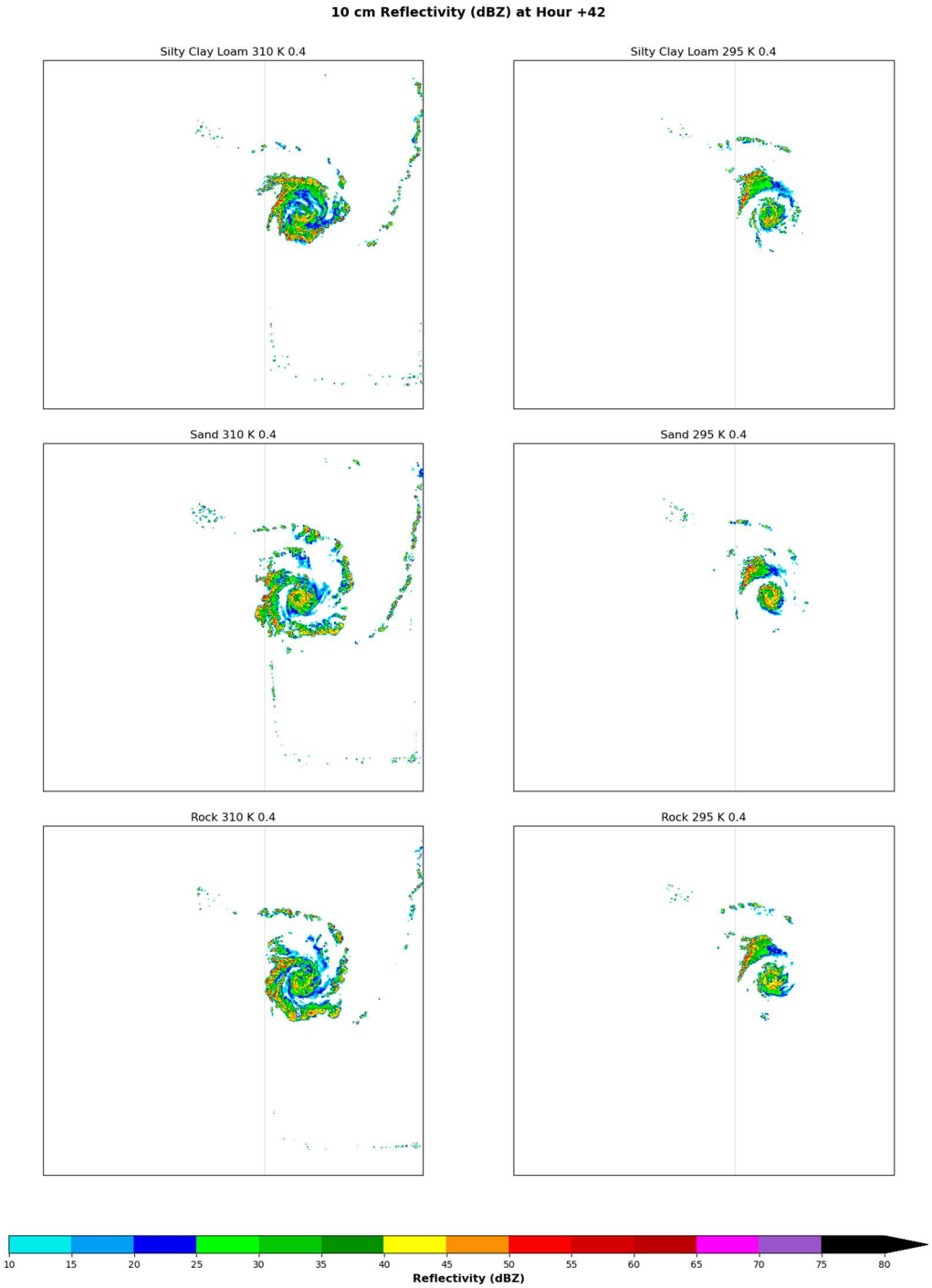

Figure 7. Simulated 10-cm reflectivity (shaded; units: dBZ) 42 h after the restart for the (left) 310-K and (right) 295-K initial soil temperature simulations for (top) silty clay loam, (middle) sand, and (bottom) rock land surfaces.

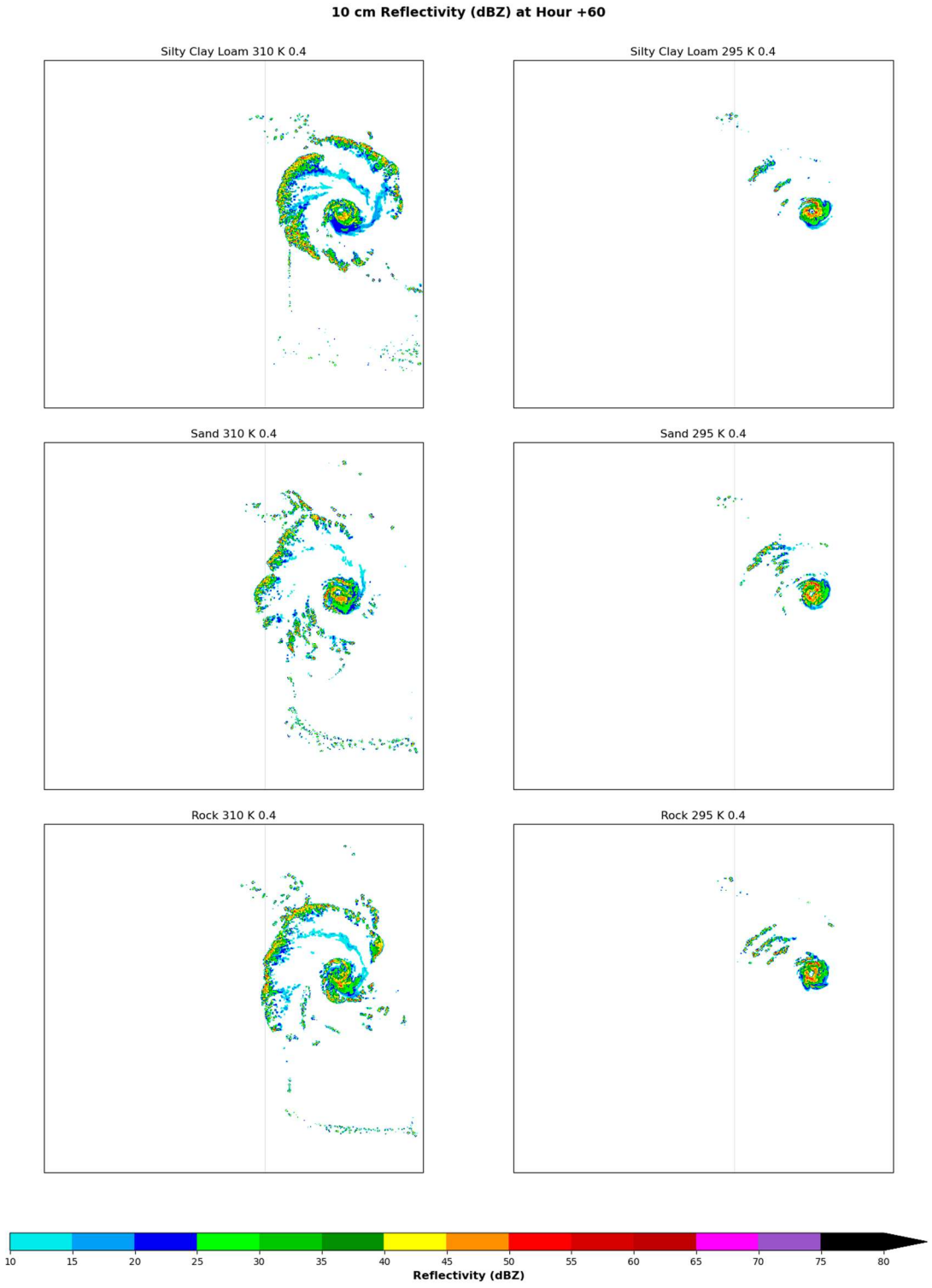

Figure 8. As in Fig. 7, except at 60 h after the restart.

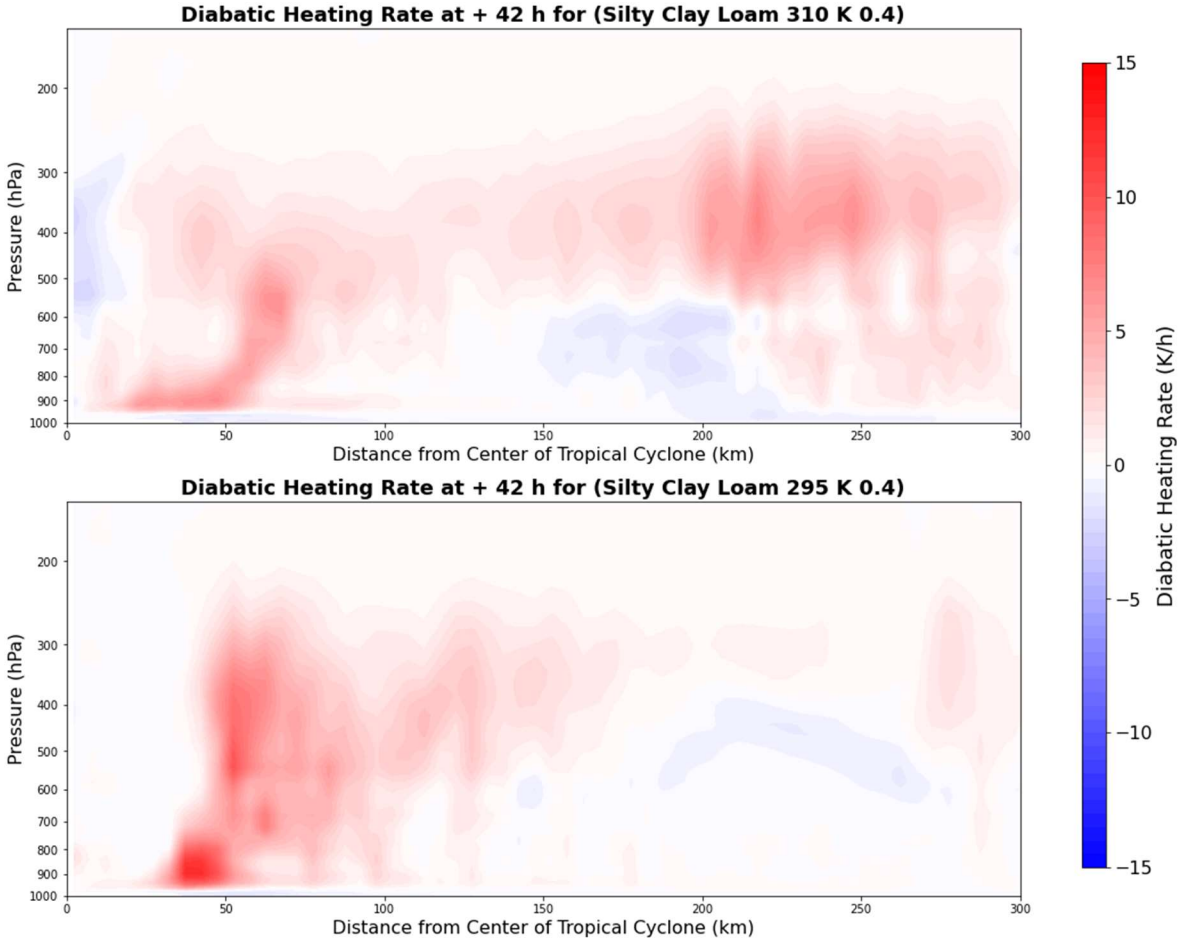

Figure 9. Radially averaged diabatic heating rate (shaded; units: K h^{-1}) at 42 h after simulation restart. The top panel is for the 310-K initial soil temperature and 0.4 initial soil moisture fraction silty clay loam simulation, whereas the bottom panel is for the 295-K initial soil temperature and 0.4 initial soil moisture fraction silty clay loam simulation.

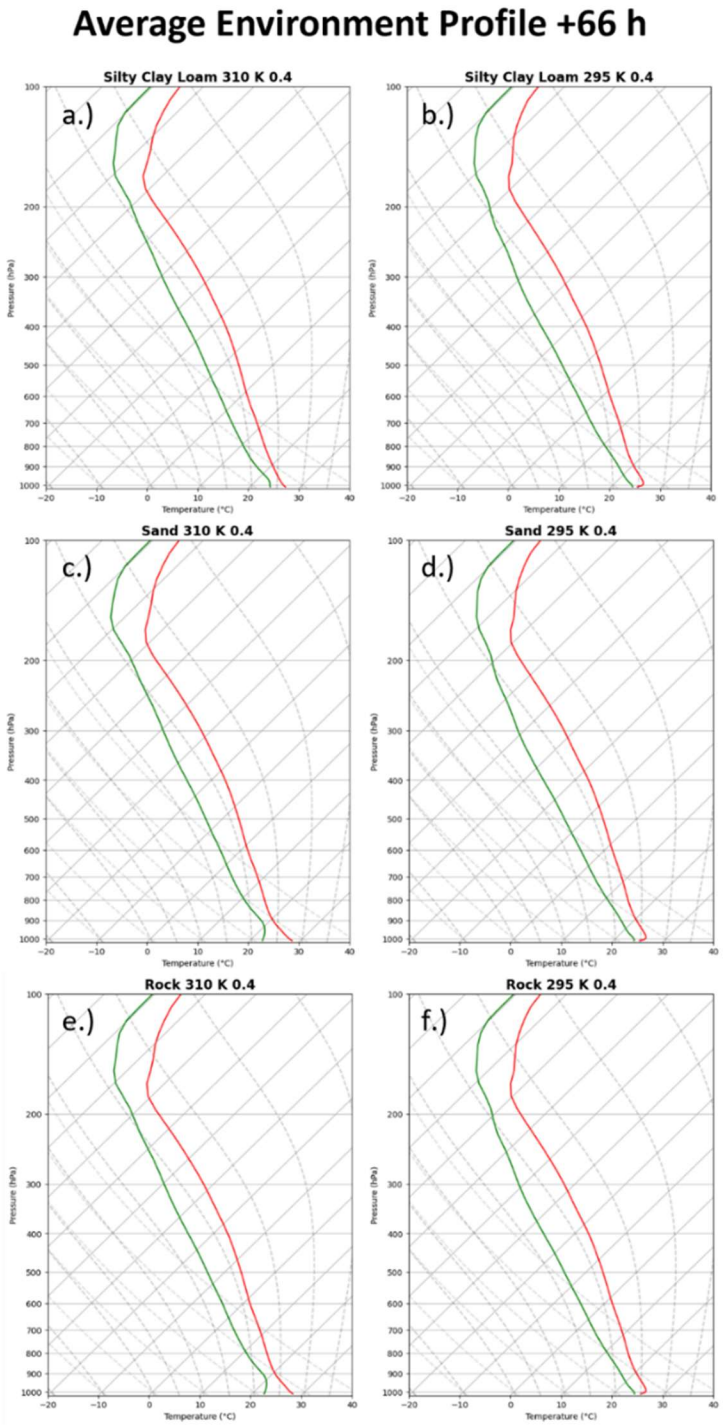

Figure 10. Average environment skew-*T*, ln-*p* diagrams (with temperature given by the red lines and dewpoint temperature given by the green lines, both in °C) for the (a,c,e) 310-K and (b,d,f) 295-K initial soil temperature simulations at 66 h after the restart. The environment is defined by the model grid points where the land surface is not ocean and where the 10-m wind is less than 10 m s^{-1} (i.e., not in proximity to the simulated tropical cyclone's center). The top, middle, and bottom rows represent the silty clay loam, sand, and rock simulations, respectively, each with an initial soil moisture fraction of 0.4.

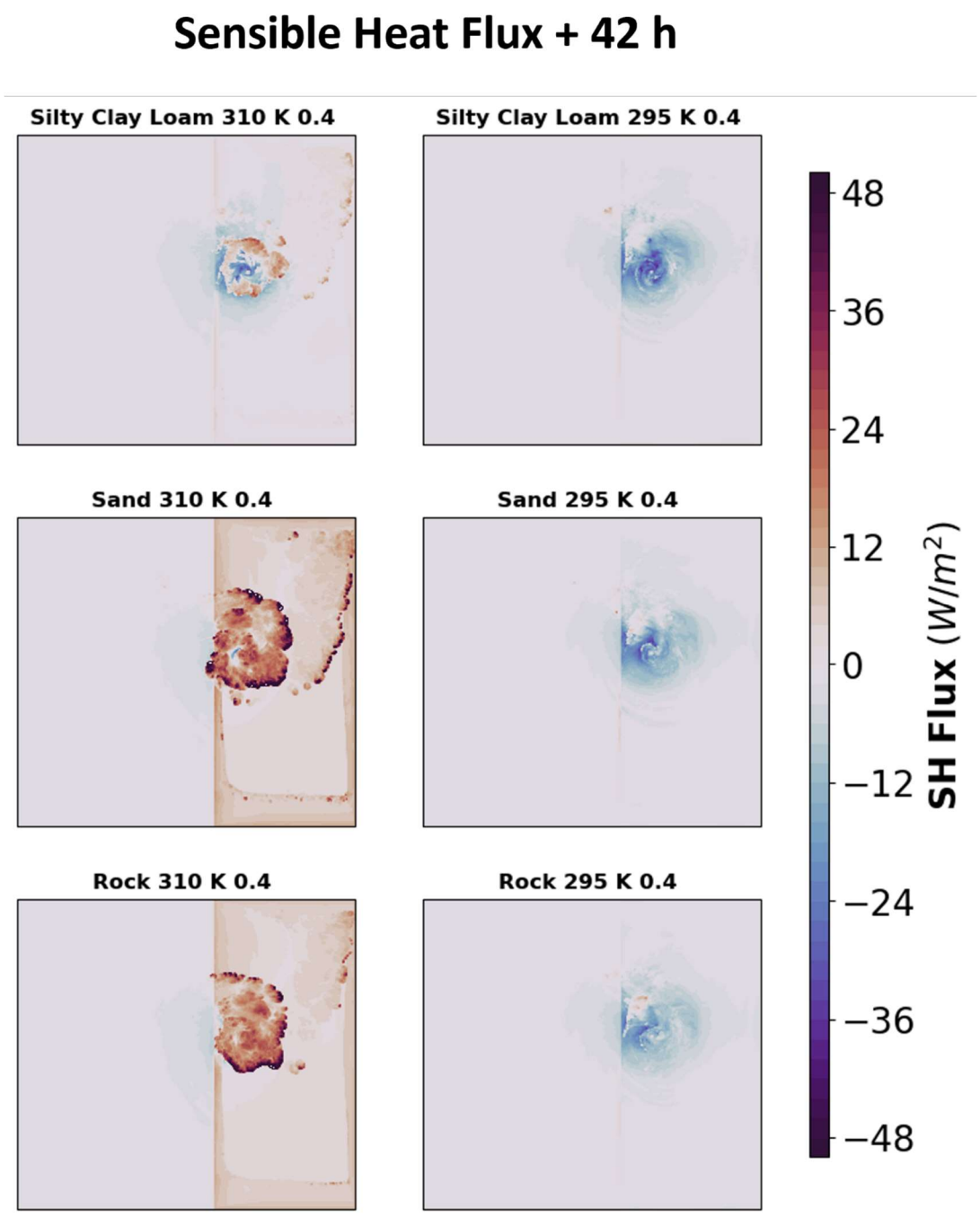

Figure 11. Surface sensible heat flux (shaded; units: W m^{-2}) for the simulations with the (left) warmest and (right) coldest initial soil temperatures for each soil type (with an initial soil moisture fraction of 0.4) at 42 h after the restart.

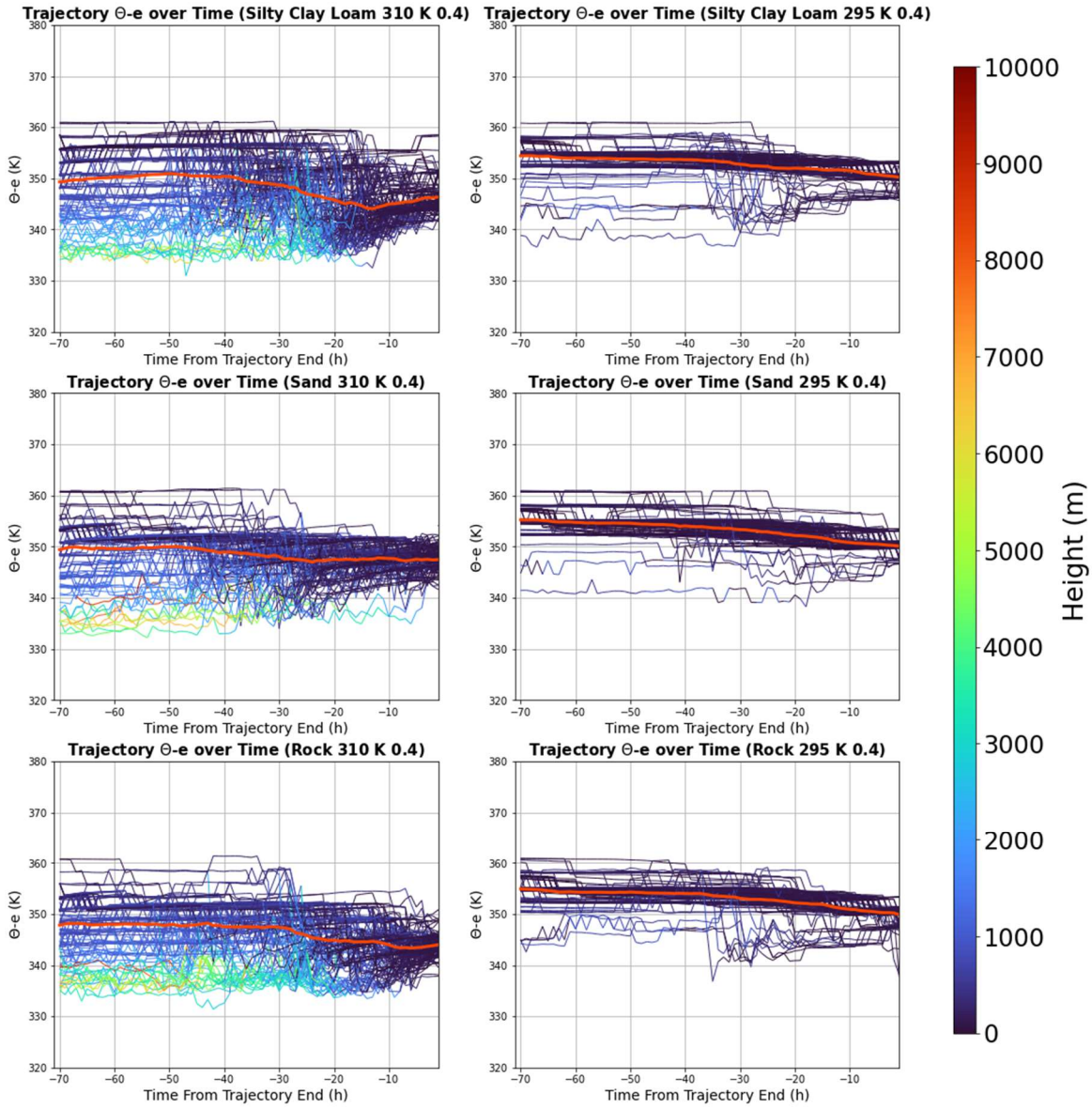

Figure 12. Along-trajectory equivalent potential temperature (*y*-axis; units: K) with time (*x*-axis, depicted as hours prior to the backward trajectories' release time). Coloring along each trajectory indicates their altitude (per the color bar at right; units: m). The red line indicates the average equivalent potential temperature for all the trajectories. The left panels indicate simulations with an initial soil temperature of 310 K, whereas the right panels indicate simulations with an initial soil temperature of 295 K. The top, middle, and bottom rows indicate simulations with silty clay loam, sand, and rock soil types. All simulations have an initial soil moisture fraction of 0.4.

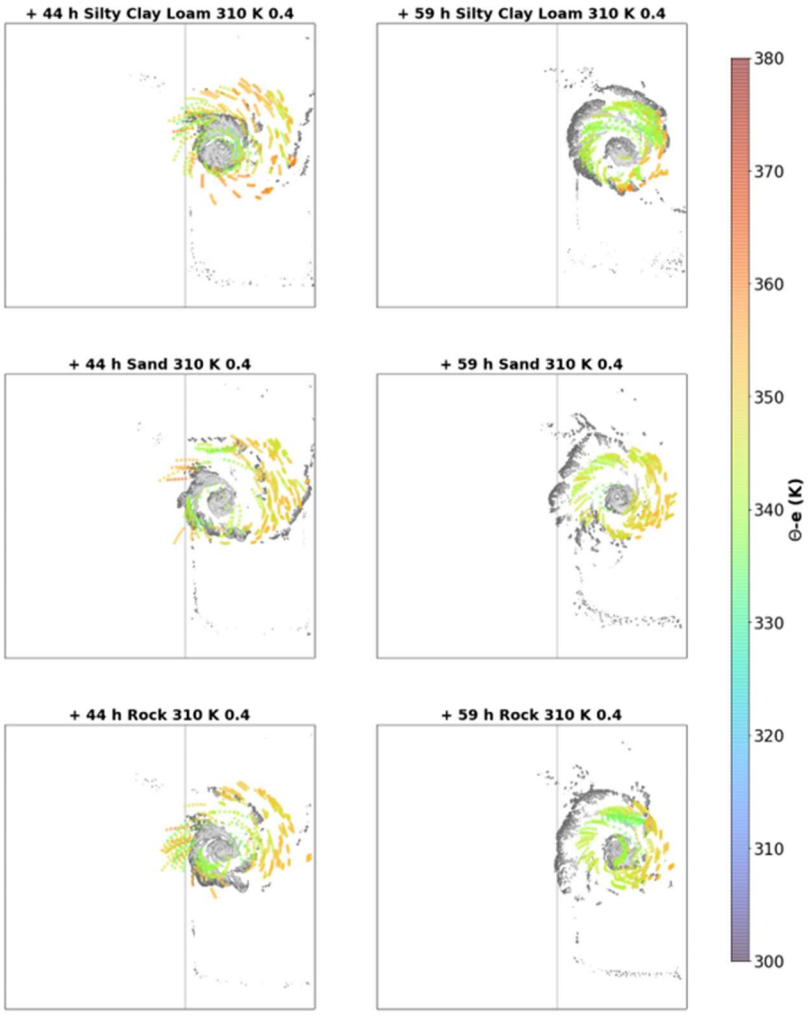

Figure 13. Six-hour trajectory paths for the simulations with the warmest initial soil temperature and largest initial soil moisture fraction. The left panels are valid at the approximate time that trajectories reach the outer rainbands (44 h after the restart) and the right panels are valid at the approximate time that all trajectories are near the surface moving towards the tropical cyclone's center (59 h after the restart). The top panels are for the silty clay loam simulations, the center panels are for the sand simulations, and the bottom panels are for the rock simulations. The coloring of the trajectory paths indicates the equivalent potential temperature (K; shaded per the color bar at right). Grey shading in all figures shows the 10-cm simulated reflectivity, with darker greys indicating larger values.

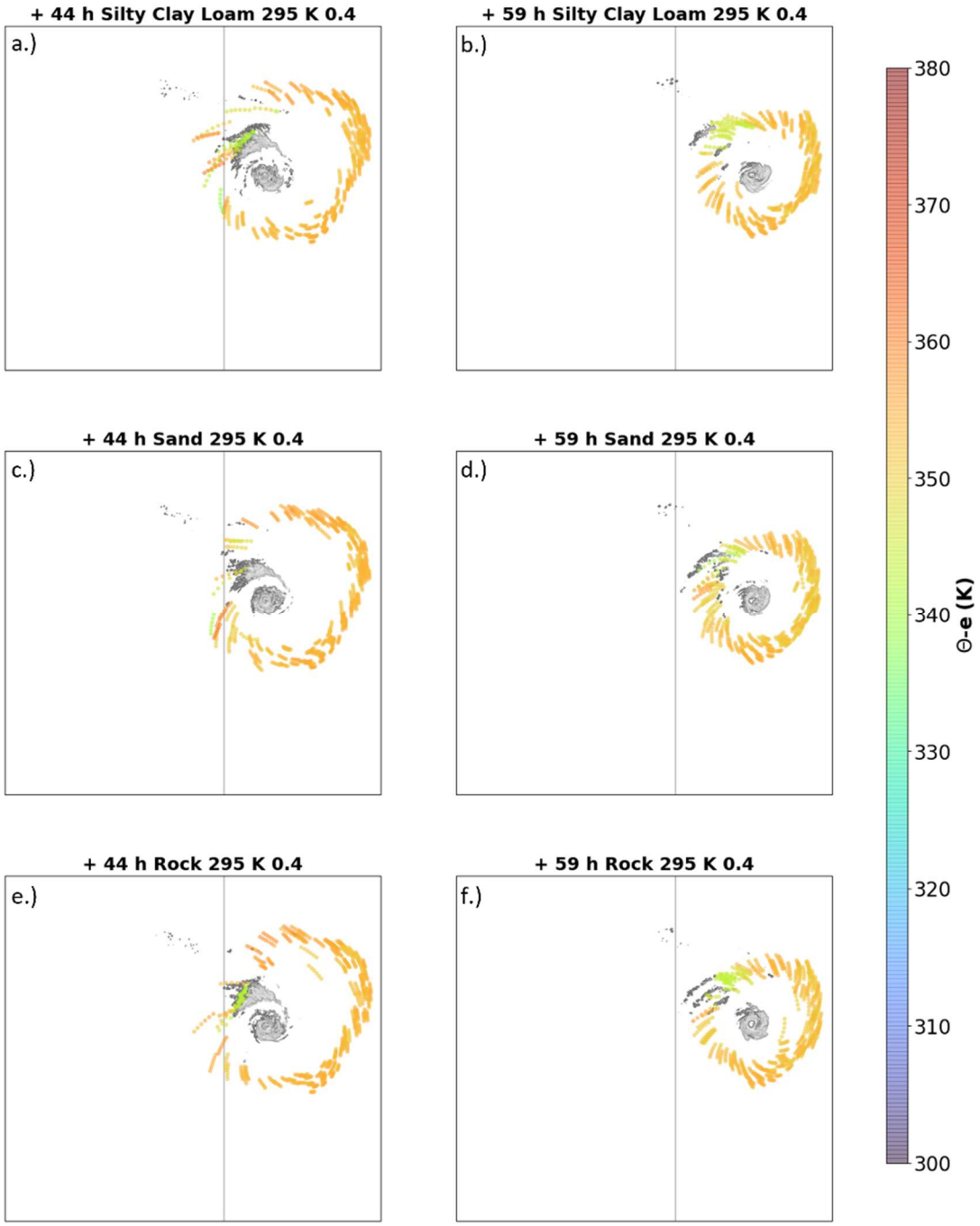

Figure 14. As in Fig. 12, except for the simulations with a 295 K initial soil temperature.

4. Discussion and Conclusions

For tropical cyclones in non-baroclinic environments in these idealized simulations with radiation omitted, a correspondence exists between simulated tropical cyclone intensity and the associated outer rainbands. Simulated tropical cyclones are most likely to maintain their intensity or to intensify inland if there are not extensive outer rainbands. The driving factor for outer rainband extent is the development of a temperature inversion near the surface in the simulations with the coldest initial soil temperatures due to a negative surface sensible heat flux between the comparatively warmer near-surface air and colder upper substrate. With the inversion preventing outer rainband formation in the simulations with colder initial soil temperatures, inflowing trajectories in these simulations are associated with larger equivalent potential temperatures and thus have more enthalpy to fuel the tropical cyclone. In the presence of outer rainbands, however, low equivalent potential temperature air from the midtroposphere is flushed into the planetary boundary layer in outer rainband downdrafts, and the underlying soil is unable to supply enough enthalpy to inflowing trajectories before they reach the tropical cyclones' centers to support overland tropical cyclone maintenance or intensification.

The temperature inversion that forms in the simulations with colder initial soil temperatures mimics a nighttime radiation inversion. During the evening, the Earth's land surface cools due to outgoing longwave radiation, in turn creating a negative surface sensible heat flux between the colder surface and warmer air immediately above the surface. Over time, this results in a nocturnal radiation inversion similar to that seen in the coldest initial soil temperature simulations in this investigation. The impact of near-surface inversions on tropical cyclones is similar to what has been found with midtroposhperic mesoscale convective vortices (MCVs) over North America, wherein deep, moist convection is confined at night to near an

MCV's center by a radiatively driven near-surface inversion at larger radii (Trier et al. 2000). Thus, overland tropical cyclone maintenance and intensification in a weakly or non-baroclinic environment appears to favor nighttime-like environments, at least in the simulations reported on in this study.

With how the inversion mechanism is created, tropical cyclone maintenance over land is more sensitive to initial soil temperature rather than to soil moisture, in sharp contrast to Emanuel et al. (2008). A weak correlation between initial soil moisture fraction and simulated tropical cyclone intensity exists in the silty clay loam simulations, however, mainly because silty clay loam's field capacity is high enough to hold enough moisture to substantially impact the surface latent heat flux. Conversely, in the sand (as considered by Emanuel et al. 2008) and rock simulations, soil moisture quickly drains out due to their low field capacities, resulting in very weak surface latent heat fluxes. One key difference between this study and Emanuel et al. (2008) is that the latter prescribed sand to either be completely dry or completely saturated, the latter of which far exceeds the soil's field capacity and thus does not represent realistic soil conditions.

The initial soil temperature also contrast with Evans et al. (2011), which focuses on surface latent heat fluxes along inflowing near-surface trajectories. In this study, the simulations in which the tropical cyclone intensifies are associated with surface latent heat fluxes along the inflowing near-surface trajectories under 75 W m^{-2}, which is well below the 150 W m^{-2} that Montgomery et al. (2009) suggests is needed to maintain a tropical cyclone. This limits any increase in near-surface moisture content along inflowing trajectories. Further, inflowing near-surface trajectories in the simulations in which a tropical cyclone maintains or increases its intensity after landfall do not experience an increase in equivalent potential temperature over

land but rather experience a small decrease in equivalent potential temperature on their way towards the tropical cyclone's center (Fig. 13). Thus, in the simulations that conducted in this study, the physical mechanisms described by Emanuel et al. (2008) and Evans et al. (2011) do not play a primary role in simulated overland tropical cyclone intensification or maintenance; rather, the primary mechanism in this investigation is the nighttime inversion mechanism described earlier.

Even though this study's results do not appear to directly support the theories of Emanuel et al. (2008) or Evans et al. (2011), they are supported by some recent investigations on overland weakly or non-baroclinic tropical cyclone maintenance and intensification. For example, two other recent investigations suggest that changing the initial soil moisture content does not have a substantial impact on tropical cyclone intensity well after landfall (Yoo et al. 2020, Hlywiak and Nolan 2021). Furthermore, some investigations have suggested that tropical cyclones overland respond to the diurnal cycle through its control of outer rainband activity (e.g., Yoo et al. 2020), with the tropical cyclone sometimes intensifying at night (Evans et al. 2011, Yoo et al. 2020). Thus, other investigations support this study's key finding of the diurnal cycle and the extent of outer rainbands playing an important role in tropical cyclone maintenance and intensification overland in weakly or non-baroclinic environments.

With this investigation being only an idealized modeling study, there are some limitations to address in the future. First and foremost, further investigation is needed to see if the nighttime inversion mechanism still holds true when radiation is included. Preliminary results with radiation parameterized suggest that initial soil moisture content plays a more important role than does the initial soil temperature in facilitating tropical cyclone maintenance due to the greater consistency in simulated soil temperatures between simulations in the presence of a diurnal

cycle. A second shortcoming is the idealized initial atmospheric state, which is set to the Dunion (2011) moist tropical sounding across the entire domain. This atmosphere is well suited for over the ocean but it does not represent atmospheric conditions over land as reliably. These simulations also do not allow for the typical spatial atmospheric variability between ocean and land. Although this approach ensures a weakly baroclinic environment devoid of large-scale horizontal temperature gradients, it also may limit the results' applicability to observed events. Future work beyond this investigation will attempt to address these shortcomings and others.

References

Anderson, T. K. and J. M. Shepherd, 2014: A global spatiotemporal analysis of inland tropical cyclone maintenance or intensification. *Int. J. Climatol*., **34**, 391–402, https://doi.org/10.1002/joc.3693.

Andersen, T. K., D. E. Radcliffe, and J. M. Shepherd, 2013: Quantifying surface energy fluxes in the vicinity of inland-tracking tropical cyclones, *J. Appl. Meteor. Climatol.*, **52**, 2797–2808, https://doi.org/10.1175/JAMC-D-13-035.1.

Arndt, D. S., J. B. Basara, R. A. McPherson, B. G. Illston, G. D. McManus, and D. B. Demko, 2009: Observations of the overland reintensification of Tropical Storm Erin (2007). *Bull. Amer. Meteor. Soc.*, **90**, 1079–1093, https://doi.org/10.1175/2009BAMS2644.1.

Chen, F. and J. Dudhia, 2001: Coupling an advanced land surface–hydrology model with the Penn State–NCAR MM5 modeling system. Part I: model implementation and sensitivity. *Mon. Wea. Rev*., **129**, 569–585, https://doi.org/10.1175/1520-0493(2001)129<0569:CAALSH>2.0.CO;2.

Chen, J., and D. R. Chavas, 2020: The transient responses of an axisymmetric tropical cyclone to instantaneous surface roughening and drying, *J. Atmos. Sci*., **77**, 2807–2834, https://doi.org/10.1175/JAS-D-19-0320.1.

Cornell University, 2010: Competency area 2: soil hydrology AEM. [Available online at https://nrcca.cals.cornell.edu/soil/CA2/CA0212.1-3.php.]

Dahl, J. M. L., M. D. Parker, and L. J. Wicker, 2012: Uncertainties in trajectory calculations within near-surface mesocyclones of simulated supercells, *Mon. Wea. Rev*., **140**, 2959–2966, https://doi.org/10.1175/MWR-D-12-00131.1.

Davis, C. A., and S. Low-Nam, 2001: The NCAR-AFWA tropical cyclone bogussing scheme. Air Force Weather Agency (AFWA) Rep., 12 pp., available online at http://www.mmm.ucar.edu/mm5/mm5v3/tc-bogus.html.

Davis, C., and Coauthors, 2008: Prediction of landfalling hurricanes with the advanced hurricane WRF model. *Mon. Wea. Rev.*, **136**, 1990–2005, https://doi.org/10.1175/2007MWR2085.1.

Dunion, J. P., 2011: Rewriting the climatology of the tropical North Atlantic and Caribbean Sea Atmosphere. *J. Climate*, **24**, 893–908, https://doi.org/10.1175/2010JCLI3496.1.

Emanuel, K., 2018: 100 Years of progress in tropical cyclone research, *Meteor. Monographs*, **59**, 15.1–15.68, https://doi.org/10.1175/AMSMONOGRAPHS-D-18-0016.1.

Emanuel, K., J. Callaghan, and P. Otto, 2008: A hypothesis for the redevelopment of warm-core cyclones over Northern Australia. *Mon. Wea. Rev.*, **136**, 3863–3872, https://doi.org/10.1175/2008MWR2409.1.

Evans, C., R. S. Schumacher, and T. J. Galarneau, 2011: Sensitivity in the overland reintensification of tropical cyclone Erin (2007) to near-surface soil moisture characteristics. *Mon. Wea. Rev.*, **139**, 3848–3870, https://doi.org/10.1175/2011MWR3593.1.

Hill, K. A., and G. M. Lackmann, 2009: Analysis of idealized tropical cyclone simulations using the Weather Research and Forecasting Model: sensitivity to turbulence parameterization and grid spacing. *Mon. Wea. Rev.*, **137**, 745–765, https://doi.org/10.1175/2008MWR2220.1.

Hlywiak, J., and D. S. Nolan, 2021: The response of the near-surface tropical cyclone wind field to inland surface roughness length and soil moisture content during and after landfall, *J. Atmos. Sci*., **78**, 983–1000, https://doi.org/10.1175/JAS-D-20-0211.1.

Hong, S., Y. Noh, and J. Dudhia, 2006: A new vertical diffusion package with an explicit treatment of entrainment processes. *Mon. Wea. Rev*., **134**, 2318–2341, https://doi.org/10.1175/MWR3199.1.

Jiménez, P. A., J. Dudhia, J. F. González-Rouco, J. Navarro, J. P. Montávez, and E. García-Bustamante, 2012: A revised scheme for the WRF surface layer formulation. *Mon. Wea. Rev*., **140**, 898–918, https://doi.org/10.1175/MWR-D-11-00056.1.

Kellner, O., D. Niyogi, M. Lei, and A. Kumar, 2011: The role of anomalous soil moisture on the inland reintensification of Tropical Storm Erin (2007). *Nat Hazards,* **63,** 1573–1600, https://doi.org/10.1007/s11069-011-9966-6.

Kleinschmidt, Jr., E., 1951: Grundlagen einer theorie der tropischen zyklonen. *Arch. Meteor. Geophys. Bioklimatol.*, **4A**, 53–72, https://doi.org/10.1007/BF02246793.

Miltenberger, A. K., S. Pfahl, and H. Wernli, 2013: An online trajectory module (version 1.0) for the nonhydrostatic numerical weather prediction model COSMO, *Geosci. Model Dev.*, **6**, 1989–2004, https://doi.org/10.5194/gmd-6-1989-2013.

Monteverdi, J. P., and R. Edwards, 2010: The redevelopment of a warm-core structure in Erin: a case of inland tropical storm formation. *Elec. J. Severe Storms Meteor.*, **5**, 1–18, https://ejssm.org/ojs/index.php/ejssm/article/view/65/59.

Montgomery, M. T., V. S. Nguyen, J. Persing, and R. K. Smith, 2009: Do tropical cyclones intensify by WISHE? *Quart. J. Roy. Meteor. Soc.*, **135**, 1697–1714, https://doi.org/10.1002/qj.459.

National Hurricane Center, 2021: The Saffir-Simpson hurricane wind scale. [Available online at https://www.nhc.noaa.gov/pdf/sshws.pdf.]

Ooyama, K., 1969: Numerical simulation of the life cycle of tropical cyclones. *J. Atmos. Sci.*, **26**, 3–40, https://doi.org/10.1175/1520-0469(1969)026<0003:NSOTLC>2.0.CO;2.

Powell, M. D., 1990: Boundary layer structure and dynamics in outer hurricane rainbands. Part II: downdraft modification and mixed layer recovery. *Mon. Wea. Rev.*, **118**, 918–938, https://doi.org/10.1175/1520-0493(1990)118%3C0918:BLSADI%3E2.0.CO;2.

Riehl, H., 1950: A model of hurricane formation. *J. Appl. Phys.*, **21**, 917–925, https://aip.scitation.org/doi/10.1063/1.1699784.

Shamarock, W. C., and Coauthors, 2019: A description of the Advanced Research WRF version 4. *NCAR Tech. Note*, NCAR/TN-556+STR, 162 pp.

Shen, W., I. Ginis, and R. E. Tuleya, 2002: A numerical investigation of land surface water on landfalling hurricanes. *J. Atmos. Sci.*, **59**, 789–802, https://doi.org/10.1175/1520-0469(2002)059<0789:ANIOLS>2.0.CO;2.

Thompson, G., P. R. Field, R. M. Rasmussen, and W. D. Hall, 2008: Explicit forecasts of winter precipitation using an improved bulk microphysics scheme. Part II: implementation of a new snow parameterization. *Mon. Wea. Rev*., **136**, 5095–5115, https://doi.org/10.1175/2008MWR2387.1.

Trier, S. B., C. A. Davis, and J. D. Tuttle, 2000: Long-lived mesoconvective vortices and their environment. Part I: Observations from the central United States during the 1998 warm season. *Mon. Wea. Rev.*, **128**, 3376–3395, https://doi.org/10.1175/1520-0493(2000)128<3376:LLMVAT>2.0.CO;2.

Tuleya, R. E., 1994: Tropical storm development and decay: sensitivity to surface boundary conditions. *Mon. Wea. Rev.*, **122**, 291–304, https://doi.org/10.1175/1520-0493(1994)122<0291:TSDADS>2.0.CO;2.

Yoo, J., J. A. Santanello, Jr., M. Shepherd, S. Kumar, P. Lawston, and A. M. Thomas, 2020: Quantification of the land surface and brown ocean influence on tropical cyclone intensification over land, *J. Hydrometeor.,* **21**, 1171–1192, https://doi.org/10.1175/JHM-D-19-0214.1.